

# A REAL-TIME ALGORITHM FOR TIME DECODING MACHINES

Aurel A. Lazar

Dept. of Electrical Engineering  
Columbia University,  
New York, NY 10027, USA  
aurel@ee.columbia.edu

Ernő K. Simonyi

Ministry of Defense Electronics,  
Logistic and Property Management Co.,  
H-1101 Budapest, Hungary,  
simonyi.erno@hmei.hu

László T. Tóth

Dept. of Telecom. and Media  
Informatics, Budapest Univ. of  
Technology and Economics,  
H-1117 Budapest, Hungary  
tothl@tmit.bme.hu

## ABSTRACT

Time-encoding is a real-time asynchronous mechanism of mapping the information contained in the amplitude of a bandlimited signal into a time sequence. Time decoding algorithms recover the signal from the time sequence. Under an appropriate Nyquist-type rate condition the signal can be perfectly recovered. The algorithm for perfect recovery calls, however, for the computation of a pseudo-inverse of an infinite dimensional matrix. We present a simple algorithm for local signal recovery and construct a stitching algorithm for real-time signal recovery. We also provide a recursive algorithm for computing the pseudo-inverse of a family of finite-dimensional matrices.

## 1. INTRODUCTION

Time-encoding is a real-time asynchronous mechanism of mapping the amplitude information of a bandlimited signal  $x(t)$ ,  $t \in \mathbb{R}$ , into a time sequence  $(t_k)$ ,  $k \in \mathbb{Z}$ , where  $\mathbb{R}$  and  $\mathbb{Z}$  denote the sets of real numbers and integers, respectively. A Time Encoding Machine (TEM) is a realization of such an asynchronous algorithm. The first example of a TEM (see [7] and the references therein), also shown in Figure 1, was an asynchronous sigma-delta modulator. Other TEMs include integrate-and-fire neurons [8] and frequency modulators (combined with a zero crossings detector) [7]. The major advantage of time encoding as opposed to traditional analog-to-digital conversion is that TEMs can be implemented by simple and robust nonlinear analog VLSI circuits with low power consumption [10], [5]. Under Nyquist-type rate conditions,  $x(t)$  can be reconstructed from the  $t_k$ 's by algorithms commonly referred to as Time Decoding Machines (TDMs). Although methods used in frame theory [2], [6], and irregular sampling [3], are needed to establish these conditions [7], [8], recovery algorithms are often easy to formulate and usually call for solving consistent but (typically) ill-conditioned infinite-dimensional linear equations.

## 2. PROBLEM FORMULATION

The TEM and the associated TDM discussed in [7] is used to illustrate our work. Figure 1 shows a TEM consisting of an integrator and a Schmitt trigger in a negative-feedback, where  $\kappa$ ,  $\delta$  and  $b$  are circuit parameters,  $c$  and  $\Omega$  are the amplitude and (angular) frequency bound, respectively, of the input signal  $x(t)$  with Fourier transform  $X(\omega)$ . As shown, the zero-crossings of the asynchronous binary output  $z(t)$  determine the  $t_k$ 's subsequently referred to as the trigger times.

A simple analysis of the TEM in Figure 1 gives [7]

$$\int_{t_k}^{t_{k+1}} x(t) dt = (-1)^k (2\kappa\delta - b(t_{k+1} - t_k)), \quad (1)$$

for all  $k \in \mathbb{Z}$ . The TDM algorithm of [7] can be found by assuming that  $x(t)$  is expressed as

$$x(t) = \sum_{\ell \in \mathbb{Z}} c_\ell g(t - s_\ell) \quad \text{with} \quad s_\ell = \frac{t_\ell + t_{\ell+1}}{2}, \quad (2)$$

where  $g(t) = \sin \Omega t / (\pi t)$  is the impulse response of an ideal lowpass filter (LPF) with cutoff frequency  $\Omega$ , and the coefficients  $c_\ell$  are to be found. Substituting (2) into (1) gives:

$$\sum_{\ell \in \mathbb{Z}} \underbrace{c_\ell}_{[\mathbf{c}]_\ell} \underbrace{\int_{t_k}^{t_{k+1}} g(t - s_\ell) dt}_{[\mathbf{G}]_{k,\ell}} = \underbrace{(-1)^k (2\kappa\delta - b(t_{k+1} - t_k))}_{[\mathbf{q}]_k}$$

With the definitions of the matrix  $\mathbf{G}$  and, vectors  $\mathbf{q}$  and  $\mathbf{c}$  introduced above, the unknown  $\mathbf{c}$  verify the linear equations  $\mathbf{G}\mathbf{c} = \mathbf{q}$ . It can be shown [7] that the representation in equation 2 leads to perfect reconstruction if the Nyquist-type condition  $2\kappa\delta/(b - c) < \pi/\Omega$  is satisfied. Note that  $\mathbf{G}$ ,  $\mathbf{q}$  and  $\mathbf{c}$  have infinite dimensions.

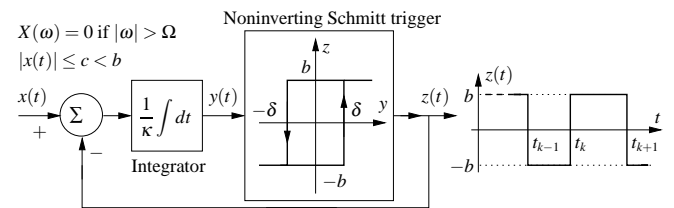


Figure 1: TEM based on the Asynchronous Sigma/Delta Modulator.

Our goal is to derive a simple real-time algorithm that recovers the signal  $x(t)$ ,  $t \in \mathbb{R}$ , from the time sequence  $(t_k)$ ,  $k \in \mathbb{Z}$ . The algorithm presented here is based on finding good approximations of the signal on short (in part) overlapping time intervals and then “stitching” these approximations together. We provide a stitching procedure based on the choice of a *variable* time window and three parameters that give the designer of the algorithm substantial flexibility for addressing problems arising in practice. We also investigate recursive algorithms for computing the pseudo-inverse of  $\mathbf{G}$  given data on finite time intervals.

The rest of this paper is organized as follows. In section 2.1 we introduce a local covering of  $\mathbf{G}$  and investigate the local recovery of  $x(t)$  using a finite number of trigger times.

The stitching real-time recovery algorithm is presented in section 3. A recursive algorithm for computing the pseudo-inverse of the covering is described in section 4.

## 2.1 Reduction to a Finite Dimensional Covering

In what follows we assume that only a finite set of trigger times is available for signal reconstruction. Given  $m$  and  $L$ , this set is denoted by  $\{t_m, t_{m+1}, \dots, t_{m+L}\}$ . Based on this set we define the vector  $\mathbf{q}_{m,L}$  with  $L$  elements and the  $L$  by  $L$  matrix  $\mathbf{G}_{m,L}$  as

$$\begin{aligned} [\mathbf{q}_{m,L}]_{k-m+1} &= (-1)^k (2\kappa\delta - b(t_{k+1} - t_k)) \\ [\mathbf{G}_{m,L}]_{k-m+1, \ell-m+1} &= \int_{t_k}^{t_{k+1}} g(t - s_\ell) dt, \end{aligned} \quad (3)$$

for all  $k, \ell = m, m+1, \dots, m+L-1$ .  $\mathbf{G}_{m,L}, m \in \mathbb{Z}$ , defines a local covering of length  $L$  of  $\mathbf{G}$ .

An approximation for  $x(t)$  (see also equation (2)) is given by

$$x_{m,L}(t) = \sum_{\ell=m}^{m+L-1} [\mathbf{c}_{m,L}]_{\ell-m+1} g(t - s_\ell), \quad (4)$$

where  $\mathbf{c}_{m,L}$  is an  $L$  dimensional vector that is obtained by solving the equation  $\mathbf{G}_{m,L} \mathbf{c}_{m,L} = \mathbf{q}_{m,L}$ . Since  $\mathbf{G}_{m,L}$  is typically ill-conditioned, the minimum-norm solution is obtained by

$$\mathbf{c}_{m,L} = \mathbf{G}_{m,L}^+ \mathbf{q}_{m,L}, \quad (5)$$

where  $\mathbf{G}_{m,L}^+$  denotes the pseudo-inverse of  $\mathbf{G}_{m,L}$  [1]. As the example in Sec. 2.2 illustrates,  $x_{m,L}(t)$  created by using the trigger times within  $[t_m, t_{m+L}]$  can accurately approximate  $x(t)$  in a reduced range  $[t_{m+M}, t_{m+L-M}]$  for some given  $M$  (typically ranging between 2 and 5 in our simulations). (This locality property has also been investigated in [4].) Outside this range the approximation is poor. The approximation can be quantified by the error function  $e_{m,L}(t)$  and its RMS value  $\mathcal{E}_{m,L,M}$  in dB defined as

$$\begin{aligned} e_{m,L}(t) &= x(t) - x_{m,L}(t) \\ \text{and } \mathcal{E}_{m,L,M} &= 10 \lg \left( \frac{\int_{t_{m+M}}^{t_{m+L-M}} e_{m,L}^2(t) dt}{t_{m+L-M} - t_{m+M}} \right), \end{aligned} \quad (6)$$

respectively, with  $t \in [t_{m+M}, t_{m+L-M}]$ . An extensive analysis of the dual problem of reconstructing bandlimited-signals from irregular samples appears in [9].

## 2.2 Example

With  $c = 0.3$  and  $\Omega = 2\pi \times 40$  krad/s, the input signal is shown by the dashed trace of Figure 3. It was created as a sum 20 sinusoids with amplitudes, frequencies, and phases randomly selected within  $[-1, 1]$ ,  $[0, \Omega/(2\pi)]$ , and  $[0, 2\pi]$ , respectively. The resulting signal was finally scaled such that  $|x(t)| \leq c$ . In numerical simulations 123 trigger times were determined with high accuracy together with  $y(t)$  and  $z(t)$  as shown in Figure 2. For different values of  $m$  and  $L$  the approximations and the corresponding RMS errors were evaluated with the equations (3)-(6). As seen in Figure 3, the accuracy of the approximation can be improved by increasing  $L$ .

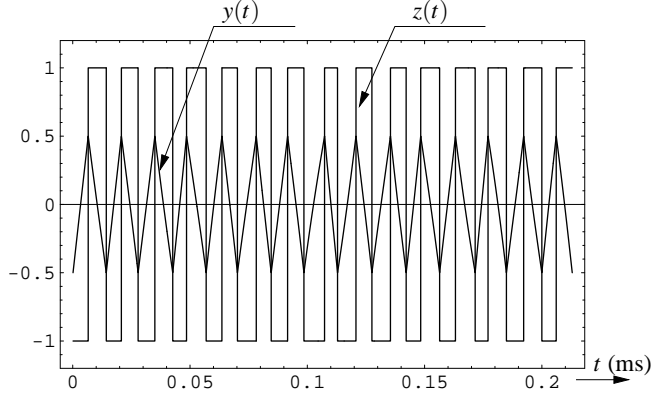


Figure 2: Simulated TEM signals  $y(t)$  and  $z(t)$  of Figure 1.

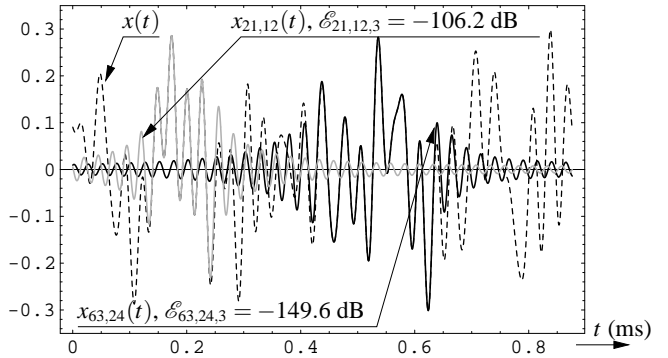


Figure 3: Input signal  $x(t)$  and two approximations in different intervals and over different lengths.

## 3. A STITCHING ALGORITHM FOR SIGNAL RECOVERY

As the example above shows, accurate approximations can be achieved within finite time intervals. Thus, a reasonable approach for the overall signal reconstruction is to (i) carry out approximations in different intervals using (3)-(6), (ii) cut out the accurate parts by appropriate windows forming a partition of unity, and finally (iii) sum up the windowed approximations.

The window  $w = w_n(t, L, M, K)$  is a key design parameter. In addition to time and time shift, and the parameters  $L$  and  $M$ , the window depends on a new parameter  $K$ .  $K$  specifies the number of trigger times over which consecutive windows overlap. When overlapping, the windows sum up to one. This condition amounts to a partition of unity that arises in multiresolution analysis. Note however, that while  $K$  is fixed, the length of the time window is variable. Formally, defining

$$J = L - 2M - K, \quad \tau_n = t_{nJ+M}, \quad \sigma_n = t_{nJ+M+K} \quad (7)$$

the overall signal approximation is given by

$$x_{L,M,K}(t) = \sum_{n \in \mathbb{Z}} w_n(t, L, M, K) x_{nJ,L}(t) \quad (8)$$

with windows

$$w_n(t, L, M, K) = \begin{cases} 0 & \text{if } t \notin (\tau_n, \sigma_{n+1}] \\ \theta_n(t) & \text{if } t \in (\tau_n, \sigma_n] \\ 1 & \text{if } t \in (\sigma_n, \tau_{n+1}] \\ 1 - \theta_{n+1}(t) & \text{if } t \in (\tau_{n+1}, \sigma_{n+1}] \end{cases}, \quad (9)$$

where the  $\theta_n(t)$ 's are appropriately chosen (otherwise arbitrary) functions. With  $t_0 = 0$ ,  $L = 8$ ,  $M = 2$ , and  $K = 1$  an illustration is shown in Figure 4. The lowest trace demonstrates that the windows so defined indeed form a partition of unity.

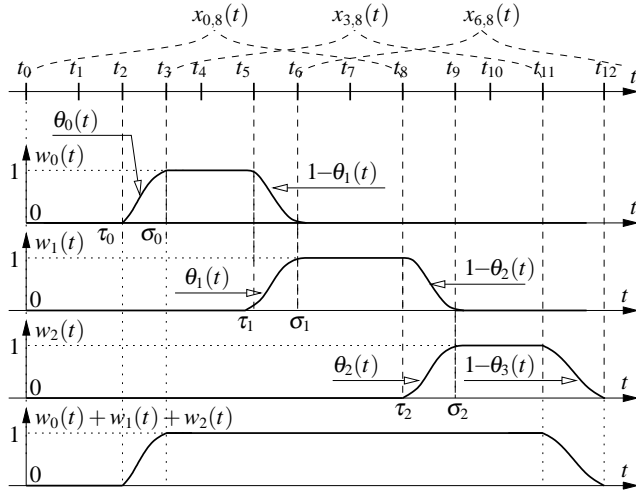


Figure 4: Illustration of the proposed reconstruction with  $t_0 = 0$ ,  $L = 8$ ,  $M = 2$ , and  $K = 1$  ( $J = 3$ ).

The bandwidth of  $x_{L,M,K}(t)$  certainly exceeds  $\Omega$ . In particular, denoting the Fourier transform of  $w_n(t, L, M, K)$  by  $W_n(\omega, L, M, K)$ , let  $\Omega_w$  be such that  $W_n(\omega, L, M, K) \simeq 0$  for all  $n \in \mathbb{Z}$  whenever  $|\omega| > \Omega_w$ . Since the bandwidth of  $x_{nJ,L}(t)$  is  $\Omega$ , (see (4)) the bandwidth of the product  $x_{nJ,L}(t)w_n(t, L, M, K)$  in (8), and thus that of  $x_{L,M,K}(t)$  is  $\Omega + \Omega_w$ . Increasing  $L$  not only improves the accuracy of the reconstruction (see Figure 3), but broadens  $w_n(t)$  in the time domain, and hence decreases  $\Omega_w$ . Note that the enlarged size and decreased conditioning of  $\mathbf{G}_{nJ,L}$  increases the computational load for calculating the pseudo-inverses  $\mathbf{G}_{nJ,L}^+$ .

By appropriately choosing  $\theta_n(t)$  in (9)  $\Omega_w$  can be decreased for fixed  $L$  and  $M$ . For example, both  $\theta_n(t)$  and its derivative becomes continuous and a good frequency localization for  $W_n(\omega, L, M, K)$  can be achieved by using:

$$\theta_n(t) = \sin^2\left(\frac{\pi}{2} \cdot \frac{t - \tau_n}{\sigma_n - \tau_n}\right). \quad (10)$$

The overall reconstruction error can be quantified by the error function  $e_{L,M,K}(t)$  and its RMS value in dB defined as

$$e_{L,M,K}(t) = x(t) - x_{L,M,K}(t) \quad (11)$$

$$\text{and } \tilde{\mathcal{E}}_{L,M,K} = 10 \lg \left( \frac{\int_{T_{\min}}^{T_{\max}} e_{L,M,K}^2(t) dt}{T_{\max} - T_{\min}} \right),$$

respectively, where  $t \in [T_{\min}, T_{\max}]$ . Here  $T_{\max}$  and  $T_{\min}$  are appropriate simulation-dependent bounds.

Passing  $x_{L,M,K}(t)$  through a lowpass filter with cutoff-frequency  $\Omega$  restores the original bandwidth of the input signal. If digital signal processing is required on the reconstructed signal, the samples  $x_{L,M,K}(nT_s)$ ,  $T_s \leq \pi/(\Omega + \Omega_w)$ , can be processed by a discrete-time LPF with (digital) cutoff frequency  $\pi/(1 + \Omega_w/\Omega)$ . Since the reconstruction error spreads over the range  $\omega \in (-\Omega_w - \Omega, \Omega_w + \Omega)$ , lowpass filtering in either analog or discrete-time domain further improves the overall accuracy. If  $h[k]$  and  $*$  denote the filter's impulse response and convolution in discrete-time, respectively, the error sequence and its RMS value in [dB] given by

$$\tilde{e}_{L,M,K}[k] = x(kT_s) * h[k] - x_{L,M,K}(kT_s) * h[k]$$

$$= e_{L,M,K}(kT_s) * h[k]$$

$$\text{and } \tilde{\mathcal{E}}_{L,M,K} = 10 \lg \left( \frac{\sum_{K_{\min}}^{K_{\max}} \tilde{e}_{L,M,K}^2[k]}{K_{\max} - K_{\min} + 1} \right), \quad (12)$$

respectively, can be used to quantify the resulting accuracy. Here  $K_{\min}$  and  $K_{\max}$  are chosen such that the range  $[K_{\min}, K_{\max}]$  excludes the filter transient.

**Remark.** In (3) and (10)  $t_k$  and  $\tau_n$  monotonically increase with time. Because of potential overflow, the reconstruction algorithm cannot use these values. However, this problem can be easily dealt with. Note that  $\mathbf{q}_{m,L}$  in equation (3) depends on  $T_k = t_{k+1} - t_k$  only and  $T_k$  is bounded as  $\frac{2\kappa\delta}{b+c} < T_k < \frac{2\kappa\delta}{b-c}$  [7]. By choosing the new integration variable  $u = t - t_k$ , the elements of  $\mathbf{G}_{m,L}$  in (3) become  $\int_0^{T_k} g(u + t_k - s_\ell) du$ . Furthermore,  $t_k - s_\ell$  is bounded from above as  $t_k - s_\ell < t_{m+L} - t_m$ , and from below as  $t_k - s_\ell > t_m - t_{m+L}$ . Therefore,  $|t_k - s_\ell| < \frac{2\kappa\delta}{b-c}L$ .

Finally, the numerator  $t - \tau_n = t - t_{nJ+M}$  in (10) is bounded because the window size is zero unless  $t_{nJ+M} < t < t_{nJ+M+K}$ . Thus,

$$0 < t - t_{nJ+M} < \frac{2\kappa\delta}{b-c}K.$$

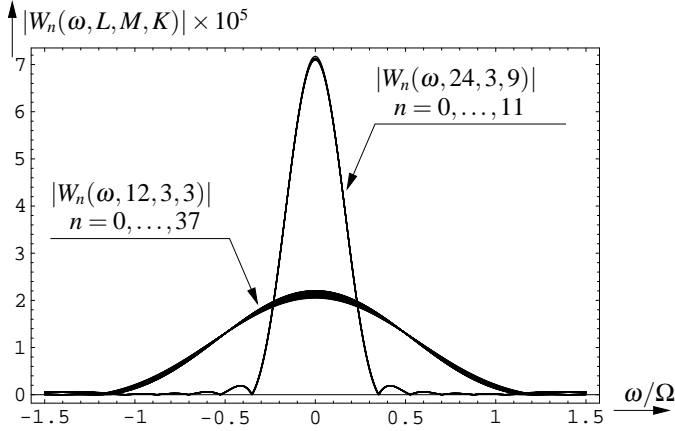
The same holds for the denominator since

$$\sigma_n - \tau_n = t_{nJ+M+K} - t_{nJ+M} < \frac{2\kappa\delta}{b-c}K.$$

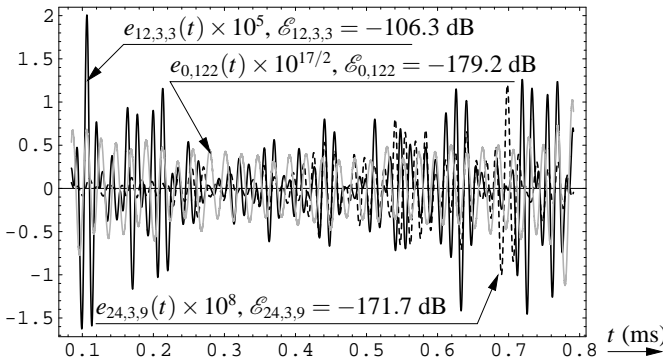
### 3.1 Example

Figure 5 shows that the windows  $|W_n(\omega, L, M, K)|$  exhibit little variation as a function of  $n$ . The windows were evaluated for  $M = 3$ , scaled in amplitude, and normalized by  $\Omega$  for different values of  $L$  and  $K$ .  $x(t)$  and the parameters of Sec. 2.2 were used for obtaining the data in Figure 6. This figure shows 3 (scaled) error signals where  $e_{12,3,3}(t)$ ,  $e_{24,3,9}(t)$ , and  $e_{24,3,9}$  were calculated by (11) with  $T_{\min} = 84.6 \mu\text{s}$  and  $T_{\max} = 791.3 \mu\text{s}$ ;  $e_{0,122}(t)$  was calculated using (6) with one single pseudo-inverse using all the available trigger times, whereas  $e_{0,122}$  was computed using (11) after replacing  $e_{L,M,K}(t)$  by  $x(t) - x_{0,122}(t)$ . As in Sec. 2.2, the reconstruction error can be decreased by increasing  $L$ . It is also noticeable that  $e_{12,3,3}(t)$  contains higher frequency components as opposed to  $e_{0,122}(t)$ .

Consider now a discrete-time filtering of the reconstructed signals. Based on Figure 5 setting  $\Omega_w = 5\Omega$  seems to be a safe choice for both sets of windows yielding  $T_s = \pi/(6\Omega) = 2.0833 \mu\text{s}$  and discrete-time cutoff frequency  $\Theta =$


 Figure 5: Two sets of frequency-domain windows with  $M = 3$ .

$\pi/6 = 0.5236$  for the filter. Figure 7 shows the impulse response and the transfer function of a simple FIR LPF with appropriate parameter settings. Using this filter and (12) on the error signals of Figure 6 with  $K_{\min} = 201$  and  $K_{\max} = 339$  (so that the range  $[K_{\min}, K_{\max}]$  contains no transient due to the LPF) gives the error sequences and the corresponding RMS values shown in Figure 8. Comparing these results with


 Figure 6: Error functions and RMS computed by (6) with  $M = 3$  and  $L$  and  $K$  of Figure 5.

those of Figure 6 it is seen that lowpass post-filtering indeed improves the accuracy. As a verification for the case of using no LPF, computing the RMS values in (12) by replacing  $\tilde{e}_{L,M,K}[k]$  by  $x(kT_s) - x_{12,3,3}(kT_s)$  and  $x(kT_s) - x_{24,3,9}(kT_s)$  gives  $-106.4$  dB and  $-171.8$  dB, respectively. These values are indeed very close to those shown in Figure 6.

Finally, note that the discrete-time signals obtained after discrete-time filtering can be decimated (downsampled). For example, in Figure 8 a decimation by 6 can be applied (data not shown).

#### 4. PSEUDO-INVERSE RECURSION OF THE COVERING

For a real-time TDM, evaluating the pseudo-inverse of  $\mathbf{G}_{m,L}$  is a critical factor in terms of both computational complexity and accuracy. Since  $L$  will be kept fixed in this section, we shall adopt the simplifying notation  $\mathbf{G}_m$ . The proposed recursion takes advantage of the fact that the consecutive ma-

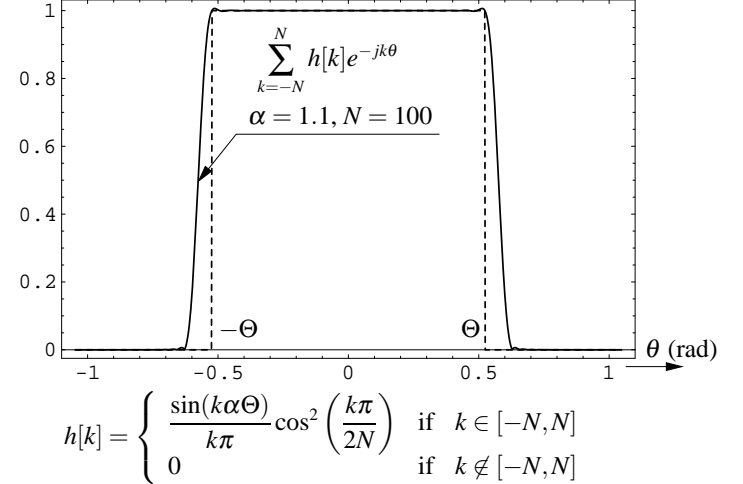


Figure 7: Discrete-time LPF impulse response and transfer function.

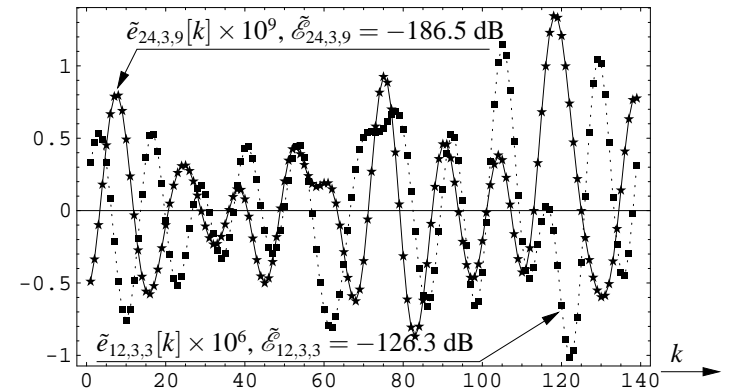


Figure 8: Scaled error sequences and discrete-time RMS errors.

trices  $\mathbf{G}_m$  and  $\mathbf{G}_{m+1}$  have a number of common elements. In particular due to (3) we have the partitions

$$\mathbf{G}_m = \begin{bmatrix} a_m & \tilde{\mathbf{a}}_m^T \\ \tilde{\mathbf{a}}_m & \mathbf{H}_m \end{bmatrix}, \quad \mathbf{G}_{m+1} = \begin{bmatrix} \mathbf{H}_m & \hat{\mathbf{b}}_m \\ \tilde{\mathbf{b}}_m^T & b_m \end{bmatrix}, \quad (13)$$

where the matrix  $\mathbf{H}_m$  represents the common part of  $\mathbf{G}_m$  and  $\mathbf{G}_{m+1}$ ,  $\hat{\mathbf{a}}_m$  and  $\hat{\mathbf{b}}_m$  are column vectors,  $\tilde{\mathbf{a}}_m^T$  and  $\tilde{\mathbf{b}}_m^T$  are row vectors, superscript  $T$  denotes transposition, and  $a_m$  and  $b_m$  are scalars. We shall denote the  $L$  by  $L$  identity matrix and its  $k$ -th column by  $\mathbf{I}$  and  $\mathbf{e}_k$ , respectively, and by  $\mathbf{P}$  the permutation matrix

$$\mathbf{P} = [\mathbf{e}_2, \mathbf{e}_3, \dots, \mathbf{e}_L, \mathbf{e}_1]. \quad (14)$$

From (13) we have

$$\mathbf{G}_{m+1} = \mathbf{P}^T \mathbf{G}_m \mathbf{P} + \mathbf{u}_m \mathbf{e}_L^T + \mathbf{e}_L \mathbf{v}_m^T, \quad (15)$$

where

$$\mathbf{u}_m = \begin{bmatrix} \hat{\mathbf{b}}_m - \tilde{\mathbf{a}}_m \\ b_m - a_m \end{bmatrix} \quad \text{and} \quad \mathbf{v}_m = \begin{bmatrix} \tilde{\mathbf{b}}_m - \tilde{\mathbf{a}}_m \\ 0 \end{bmatrix}. \quad (16)$$

Using the result of [1] (page 50, Corollary 3.1.1) in (15),  $\mathbf{G}_{m+1}^+$  can be calculated based on  $(\mathbf{P}^T \mathbf{G}_m \mathbf{P} + \mathbf{u}_m \mathbf{e}_L^T)^+$  that in

turn is determined by  $(\mathbf{P}^T \mathbf{G}_m \mathbf{P})^+$ . Since  $\mathbf{P}$  is an orthogonal matrix  $(\mathbf{P}^T \mathbf{G}_m \mathbf{P})^+ = \mathbf{P}^T \mathbf{G}_m^+ \mathbf{P}$  [1]. As a result, with input parameters  $\mathbf{G}_0^+$ ,  $\mathbf{u}_m$ ,  $\mathbf{v}_m$ ,  $\mathbf{P}$ , and  $e_L$  we have the recursion

$$\begin{aligned} \mathbf{B}_m &= \mathbf{P}^T \mathbf{G}_m^+ \mathbf{P}, \\ \beta_m &= 1 + \mathbf{e}_L^T \mathbf{B}_m \mathbf{u}_m, \\ \mathbf{A}_m &= \mathbf{B}_m - \mathbf{B}_m \mathbf{u}_m \mathbf{e}_L^T \mathbf{B}_m / \beta_m, \\ \alpha_m &= 1 + \mathbf{v}_m^T \mathbf{A}_m \mathbf{e}_L, \\ \mathbf{G}_{m+1}^+ &= \mathbf{A}_m - \mathbf{A}_m \mathbf{e}_L \mathbf{v}_m^T \mathbf{A}_m / \alpha_m, \end{aligned} \quad (17)$$

for  $m > 0$  provided that  $\beta_m \neq 0$  and  $\alpha_m \neq 0$ . Thus, apart from the initial pseudo-inverse  $\mathbf{G}_0^+$ , no further pseudo-inverse is needed to calculate  $\mathbf{G}_{m+1}^+$ . Note however that, not even this initial pseudo-inverse is needed if a short initial “transient” can be tolerated in the overall reconstruction. In particular, (13)-(16) is a formulation of the simple fact that  $\mathbf{G}_{m+1}$  is created by dropping the first row and column of  $\mathbf{G}_m$  and adding a new column and a new row. Therefore, the “effect” of any initial value, say,

$$\mathbf{G}_0 = \mathbf{G}_0^+ = \mathbf{I}, \quad (18)$$

disappears after  $L - 1$  steps. For  $m \geq L$ , the recursion in (15) gives exact values for  $\mathbf{G}_{m+1}$ , and thereby for  $\mathbf{G}_{m+1}^+$  in (17) as well. Simulation results (see Figure 9) confirm the accuracy of our recursive approach. Combining this result with the stitching algorithm discussed in Sec. 3 provides the overall real-time reconstruction algorithm.

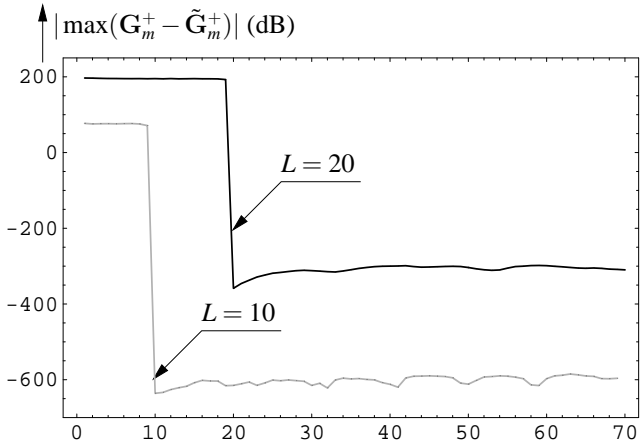


Figure 9: Comparison of the exact pseudo-inverse  $\tilde{\mathbf{G}}_m^+$  and the pseudo-inverse obtained via recursion  $\mathbf{G}_m^+$ .

## 5. CONCLUSIONS

We have presented a simple real-time recovery algorithm for time-encoded bandlimited signals. The algorithm calls for a local recovery of the signal using a finite number of trigger times. It is based on the key observation that the signal is well approximated on a core subset of the trigger times contained within the local recovery interval. By stitching the core subsets together, the signal is then recovered using a multiresolution algorithm in the time domain. The stitching algorithm presents the designer with a number of parameters that can be tuned depending on the application. The bandwidth of the recovered signal is larger than that of the original signal. Further improvements in signal recovery are achieved via postfiltering.

The recovery of a time encoded bandlimited signal from its time sequence calls for computing the pseudo-inverse of an infinite-dimensional matrix. The solution presented here is based on finding a finite local covering of the original matrix, and computing the pseudo-inverse of the covering directly as well as by a recursive method. We have implemented the two approaches for computing the pseudo-inverse both in Mathematica and in C#. The Mathematica implementation allowed us to experiment with arbitrary precision (say 40-digits accuracy). The results reported here were all based on our Mathematica implementation. The C# implementation did not use special libraries and was limited to 16-digits. For  $L = 10$  both implementations lead to an RMS reconstruction error of almost -100 dB.

In initial experiments not detailed in this paper, numerically more stable methods such as QR-decomposition and Schur-decomposition yielded an RMS reconstruction error of almost -130dB. We are currently investigating low-rank updating strategies for these methods in search of numerically more reliable recursions.

## REFERENCES

- [1] Campbell, S.L. and Meyer, C.D., Jr., *Generalized Inverses of Linear Transformations*, Dover Publications, 1979.
- [2] Christensen O., *Frames Riesz Basis, and Discrete Gabor/Wavelet Expansions*, Bulletin (New York) of the American Mathematical Society, Vol. 38, No. 3, pp. 273-291, 2001.
- [3] Feichtinger, H.G., Grochenig, G. and Strohmer, T., *Efficient Numerical Methods in Non-uniform Sampling Theory*, Numerische Mathematik, Vol. 69, pp. 423-440, 1995.
- [4] Feichtinger, H.G. and Werther, T., *Improved Locality for Irregular Sampling Algorithms*, ICASSP'2000, Istanbul, Turkey.
- [5] Kinget, P.R., Lazar, A.A. and Toth, L.T., *On the Robustness of the VLSI Implementation of a Time Encoding Machine*, Proceedings of ISCAS 2005, May 23-26, 2005, Kobe.
- [6] Kovačević J., Dragotti P.L., Goyal V.K., *Filter Bank Frame Expansions with Erasures*, Invited Paper, IEEE Transactions on Information Theory, Vol. 48, No. 6 pp. 1439-1450, June 2002.
- [7] Lazar, A.A. and Tóth L.T., *Perfect Recovery and Sensitivity Analysis of Time Encoded Bandlimited Signals*, IEEE Transactions on Circuits and Systems-I: Regular Papers, Vol. 51, No 10, pp. 2060-2073, October 2004.
- [8] Lazar, A.A., *Multichannel Time Encoding with Integrate-and-Fire Neurons*, Neurocomputing, Vol. 65-66, pp. 401-407, 2005.
- [9] Strohmer T., *Numerical Analysis of the Non-uniform Sampling Problem*, J. Comp. Appl. Math., Vol. 112, pp. 297-316, 2000.
- [10] Wei, D. and Harris J.G., *Signal Reconstruction from Spiking Neuron Models*, Proceedings of the ISCAS'04, Vol. V, pp. 353- 356, May 23-26, 2004, Vancouver, Canada.